Hindawi
Shock and Vibration
Volume 2022, Article ID 4924091, 12 pages
https://doi.org/10.1155/2022/4924091

Research Article

Analysis of Wind-Sand-Load-Induced Dynamic Response of Transmission Tower-Line Systems

Zhuoqun Zhang[1,2] **Jiashu Liu**[3,4] **Kangjie Shao**[5] **and Peng Zhang**[3]

[1]*State Grid Economic and Technological Research Institute Co Ltd, Beijing 102209, China*
[2]*State Nuclear Electric Power Planning Design & Research Institute CO. LTD, Beijing 100095, China*
[3]*Institute of Road and Bridge Engineering, Dalian Maritime University, Dalian 116023, China*
[4]*China Nuclear Power Engineering Co., Ltd, Beijing 100089, China*
[5]*China Academy of Building Research, CABR Technology CO LTD, Beijing 100013, China*

Correspondence should be addressed to Peng Zhang; peng.zhang47@dlmu.edu.cn

Received 12 October 2021; Revised 9 July 2022; Accepted 12 July 2022; Published 25 August 2022

Academic Editor: Ahmed Ibrahim

Sandstorms are a common natural phenomenon that has the potential to cause severe disruptions to civil infrastructure. However, the effect of sandstorms on transmission tower structures has not received much attention. This paper proposes the simulation of the wind-sand loads for the analysis of transmission tower structures under sandstorm excitation by superposing the wind loads and sand particle loads. The wind load is generated based on Kaimal fluctuating wind power spectrum and the harmonic superposition method, and the sand load is constructed based on the law of conservation of momentum and sandstorm classification. A transmission tower was modeled and simulated in SAP2000 to explore the dynamic response of the tower towards wind-sand loads. A comparison of wind-induced and wind-sand-induced responses shows that the structural dynamic responses of transmission towers due to the wind-sand effect are pronounced. Particularly, the maximum longitudinal displacements and axial forces increased greatly. The results showed that the sandstorm loads for transmission towers cannot be neglected, and more attention should be paid to the structural design of transmission towers to resist such loads.

1. Introduction

Power transmission tower-line systems, which are the physical structures supporting the massive national power grid of China, have seen large-scale constructions during the past decades to meet the ever-increasing energy demands associated with the rapid growing economy. Several lines composed of ultra-high voltage transmission towers have been built to convey clean energies from northwestern China to eastern China. These structures are all exposed to the harsh environmental hazards of this arid area, of which the seismic activities, strong winds, erosions, and corrosions have been carefully dealt with during the design and/or maintenance process. However, the action of sandstorms is not yet fully considered, even though they may cause severe destruction to the transmission towers, as shown in Figure 1.

The sandstorm is harmful weather that commonly occurs in the Gobi or desert regions. He et al. [1] simulate a local dust storm through a cold pool with certain vorticity. When the wind speed reaches a certain level, it can lift the top layer of sand from the ground and smash it against any obstacle that confronts it. As the wind speed increases, the destructive power grows exponentially since more particles will be driven by stronger winds.

Sandstorms have attacked many countries and regions around the world, including China, Africa, western United States among others, causing pollution of air, loss of property, and even death of humans and animals. Chinese scholars Yang et al. [2] have discovered the catalytic effect of sandstorms on PM2.5 in high-altitude areas in southern China, which is harmful to humans. American scholars Prospero et al. [3] use a spectrometer to determine the

(a) (b)

Figure 1: Facilities of the power grid subjected to a sandstorm: (a) power substation; (b) tower-line system.

source of sand particles in the atmosphere and the environmental characteristics of sandstorms.

Another hazard of the sandstorm is the moving dunes, which may cause permanent foundation displacement. Qian et al. [4] conducted experiments on building foundations under wind and sand loads, and the foundation moved under horizontal loads. Besides, the impact of subsoil flexibility should be considered in the computations. In order to analyze the hazard of the sandstorm, the sand transmission has been extensively studied during the past decades. Yang et al. [5] proposed a method to determine the velocity fields based on fluorescent tracer particles. Sherman and Li [6] compared eight sand-transport models based on field data. Experiments were conducted to reveal the relationship between the transport rate of dry sand and shear velocity [7]. The recently developed models can also be found in the following review papers [8, 9].

The hazards of sandstorms also attracted some attention from the electrical and structural engineers when they design transmission towers. One major hazard that has been intensively investigated and evaluated is the corona effect induced by the floating sand particles. Gao and Shi [10] researched the discharge mechanism of transmission lines under wind-sand load. Yunpeng et al. [11] analyzed the wires of ultra-high voltage AC lines in high-altitude areas and found that they would produce corona loss under sand and dust conditions.

There are two main types of wind involved in the engineering structure, one is large-scale winds (temperate and tropical cyclones, etc.); the other is small-scale local strong winds (typhoons, tornadoes, thunderstorms, etc.). Ishac and White [12] first proposed the basic design load of the tornado on the transmission tower-line system through investigation and research based on the relevant records of tornadoes in Ontario, Canada. Milford and Goliger [13] proposed a model formula for the probability of a tornado on the basis of previous studies, but the model did not consider the azimuth relationship between the transmission tower line, the tornado path, and the transmission tower. Savory et al. [14] established models of transient tornadoes and micro-storms, and at the same time calculated the wind speeds of the two high-strength winds over time and the loads acting on the lattice tower. And under the action of the two high-strength winds, the structure was dynamically analyzed, and the shear failure of the structure under the tornado was successfully predicted. Oliver et al. [15] assumed that the damage shape of the downburst wind accompanying a thunderstorm was a rectangle, and the transmission line was studied as a line, and established a practical model to evaluate the damage caused by the downburst wind acting on a specific length of wire. Li [16] proposed a probabilistic model for the design of transmission towers to actually and accurately simulate the wind load generated by the burst wind. This model is calibrated with previous meteorological data. Its biggest advantage is that it takes into account the influence of the size of the lower burst stream. Shehata et al. [17] established a mathematical model describing the burst wind based on the calculation data of the effective computational fluid dynamics model developed and verified by the predecessors. The geometric nonlinearity of the wire was considered, and the power transmission caused by the burst wind was analyzed and calculated.

In a related field, it is proved that the wind-driven rainfalls can severely aggravate the wind-induced vibration of high-rise or long-span structures, including suspension bridges, transmission towers. Orr and Cassar [18] use extreme wind-driven rainfall to calculate the exposure index of buildings to rainwater. Hao [19] studied the surface characteristics of large-diameter composite pillar insulators for

Table 1: Parameters of the typical intensity of sandstorms.

Parameters	Floating dust	Blowing sand	Sandstorm			
			Weak	Medium	Strong	Extra strong
Horizontal visibility	10 km	1–10 km	1 km	750 m	500 m	50 m
Wind speed (m/s)	3	6	10	15	20	25
Particle diameter (μm)	0.5	2	5	20	40	100
ρ_{TSP} (mg/m^3)[1]	0.3	1	6 (3–10)	15	25 (10–30)	100
Volume ratio	1.2	4.0	24	60	100	400

[1]ρ_{TSP} denotes the mass density of a sandstorm. TSP is the abbreviation of traveling sand particles.

transmission towers when rainfall is considered through experiments. An et al. [20] studied Windage Yaw Flashovers of transmission lines under wind and rain loads. Zhou et al. [21] studied the performance of large swing amplitude of overhead transmission lines under rain load. Compared with a raindrop, a floating sand particle contains more mass and thus has more kinetic energy at the same velocity. There are amounts of water from intensive rainfalls that flow relatively slowly from the lightweight steel structures, causing the temporary but possibly high structural mass increase, and snowstorms do not trigger such reactions.

It can be seen from the researches of the above scholars that most of the previous studies on the transmission tower-line system only analyzed the effect of other external loads such as wind load or rain load on the tower-line system and ignored the impact of sandstorms that may be caused by sand particles in the wind. Factor: in this paper, by formulating the calculation formula model of the sand storm, using the SAP2000 finite element software component linear tower-line system model, the deduced wind-sand load is applied to the tower-line system, and the straight-line tower is compared between the pure wind load and the sand load. The dynamic response of the line system: the results derived in this paper prove that sandstorms can amplify the dynamic response of power transmission towers. When the wind speed intensity of the sandstorm reaches 25 m/s, the sand load has the most obvious effect on its dynamic response amplification.

2. Wind-Sand Load Model

2.1. Sand Load Model. In order to enable the dynamic analysis of a transmission tower-line system subjected to wind-sand loads, the behavior and key parameters of sandstorms need to be characterized. The portion of a sandstorm depends on the wind speed and the general configuration of the land surface it passes. According to the existing literature and comprehensive analysis of sandstorm observation data [22], there is an obvious and direct correspondence between the sandstorm intensity and sand concentration, as shown in Table 1. It can be observed that as the wind speed increases, more sand particles can be lifted from the ground, resulting in an increasement in mass density ρ_{TSP} and volume ratio.

The momentum theorem has been widely accepted for analysis of the erosion of the sandstorm on the surface coatings of steel members [23]. According to the momentum theorem, when a sandstorm occurs, an individual sand particle can generate an impact load on the structure [24] as follows:

$$F_s(\tau) = \frac{1}{\tau}\int_0^{\tau} f(t)\mathrm{d}t = \frac{mv_1 - mv_2}{\tau}, \tag{1}$$

where m is the mass of the single sand particle; v_1 is the velocity of the sand particle before acting on the structure; v_2 is the velocity of the sand particle after acting on the structure; and $F_s(\tau)$ is the impact force generated by the individual sand particle.

Assuming that the collision between the individual sand particle and structural components is elastic, the sand particle velocity is kept constant in the opposite direction. Besides, it requires perpendicularity of element area to the wind direction.

$$v_1 = -v_2 = v_s. \tag{2}$$

Here, v_s is the average velocity of a single sand particle during the sandstorm; $F_s(\tau)$ is the impact force vector of the single sand particle acting on the transmission tower.

The impact force of a single particle of sand can be converted into a uniformly distributed load. During the collision, the shape of a single sand particle is regarded as a spherical shape. The mass of the sand grain is $m = \rho\pi d^3/6$; τ is the time when the load acts on the transmission tower; m_i ($i = 1,2,\ldots,$ N) is the weight of the i^{th} sand grain. The impact force τ of a single sand particle on the transmission tower in a unit time interval can be calculated by the following formula:

$$\begin{aligned} F_s(\tau) &= \frac{2v_s}{\tau}\sum_{i=1}^{N} m_i \\ &= \frac{1}{\tau}2v_s\frac{1}{6}\pi\sum_{i=1}^{N}\rho_i d_i^3 \\ &= \frac{1}{3\tau}\pi v_s\sum_{i=1}^{N}\rho_i d_i^3. \end{aligned} \tag{3}$$

Suppose the surface of the transmission tower is impacted by sand particles all with a specified diameter, their combined impact force can be calculated as follows:

$$F_i = F_s(\tau)n_i, \tag{4}$$

where F_i is the summation of impact forces during the time τ; n_i is the number of sand particles that impacted on the tower during the time τ.

During τ, the volume of air and sand that flows across the steel member of the transmission tower can be calculated as follows:

$$V = 2Al, \tag{5}$$

where A is the windward area exposed to the sand load; l is the distance that the wind-sand flow travels within the duration τ. So the sand load can be calculated as follows:

$$\begin{aligned} F_s &= F_i V = F_i 2Al \\ &= \frac{2}{3}\pi v_s^2 A \sum_{i=1}^{N} \rho_i n_i d_i^3. \end{aligned} \tag{6}$$

Based on the sand storm intensity (Table 1 [22]), the accumulated sand particles at a selected height can be estimated by a simplified equation as follows:

$$Q = \sum \rho_{\mathrm{TSP}} A_s V_h T. \tag{7}$$

Here, Q is the total sand accumulation amount observed at a certain height; ρ_{TSP} denotes the sand flow density of a specific wind speed (as listed in Table 1); A_s is the inlet area of sand collection equipment of the sediment observation system; V_h is the velocity of the sand particle; and T is the sampling interval of the actuation duration.

Equation (6) and (7) can be manipulated as follows:

$$\sum \rho_{TSP} A_s v_s T = \frac{1}{6}\pi \sum_{i=1}^{N} \rho_i n_i d_i^3 T A v_s. \tag{8}$$

Suppose the unit area of the transmission tower section is A, the windward area of the round steel pipe is the vertical projection of the round steel pipe under the action of wind speed, and the diameter projected on the Z-axis is the area corresponding to the round steel pipe. The total weight of steel used in the transmission tower is W, the section thickness is T, and the weight density of angle steel or steel pipe is γ, then the area A is

$$A = \frac{W}{T\gamma}. \tag{9}$$

Therefore, the final calculation formula of sand load related to sand storm concentration, sand speed, and sand load's action area is:

$$F_s(t) = 4\rho_{\mathrm{TSP}} v_s(t)^2 A. \tag{10}$$

Here, $F_s(t)$. is the sand load, v_S is the average velocity of a single sand particle; ρ_{TSP} is sand particle concentration in a unit volume, and A is the area acted on by the sand load.

2.2. Wind Load Model. The calculation of the dynamic wind load of the transmission tower-line adopts the bridge quasi-steady aerodynamic formula. When the MATLAB software is used to calculate the time history curve of the dynamic wind load of the transmission tower, the calculation formula of the wind speed changing with time at the nodes of the transmission tower structure is:

$$V(z,t) = \overline{V}(z) + V_f(z,t). \tag{11}$$

In this equation, $\overline{V}(z)$ is the average wind speed at height z; $V_f(z,t)$ denotes the fluctuating wind speed at height h. In this paper, the power transmission tower system uses a logarithmic-based wind profile.

$$\overline{V}(z) = \frac{1}{k} u_* \ln\left(\frac{z}{z_0}\right). \tag{12}$$

Here k is the Karman constant, which is an empirical coefficient introduced by von Karman's assumption of the relationship between the mixing length and the velocity profile. The measured value of the laboratory and the surface layer of the atmosphere is between 0.35 and 0.43. In recent years, 0.40 is considered to be more reasonable. In (12), z_0 = 0.2m is the ground roughness length, and u_* is the friction speed.

In addition, Kaimal considers the variation of the turbulence power spectrum with height in the atmospheric turbulence movement, and its longitudinal turbulence power spectrum expression is:

$$S_u(f) = \frac{200K\overline{V_{10}}^2}{f} \times \frac{x}{(1+50x)^{5/3}}, \tag{13}$$

where $x = hf/\overline{V_{10}}$ is the dimensionless Monin coordinate. h is the height of the simulation point, and f is the frequency of fluctuations in the wind.

The harmony superposition method is a discrete numerical method to simulate the steady random process. An arbitrary signal can be decomposed into a series of sinusoidal waves with different frequencies and amplitudes through the discrete Fourier transform. The time series describing the fluctuating wind velocity can be regarded as a stochastic process and can be characterized by its power spectrum. When $N \longrightarrow \infty$, with the theory presented by Shinozuka [25], the fluctuating wind velocity time series $\mu_i(t)$ can be modeled by

$$\begin{aligned} u_i(t) &= \sum_{l=1}^{i} \sum_{k=1}^{N} \left|H_{il}(\omega_k)\right| \sqrt{2\Delta\omega_k} \cos\left[\omega_k t - \theta_{il}(\omega_k) + \varphi_{lk}\right], \\ i &= 1, 2, \ldots, m, \end{aligned} \tag{14}$$

where i is the number of calculation points, H_{il} is obtained from the Cholesky decomposition of the wind cross-spectral density matrix, $\theta_{il}(\omega)$ is the argument of $H_{il}(\omega)$, and φ_{lk} denotes the uniformly distributed random numbers in [0, 2π]. Integrate the density in the power spectrum:

$$\int_0^{\omega_u} S(\omega) d\omega = (1-\varepsilon) \int_0^{\infty} S(\omega) d\omega, \tag{15}$$

where ω_u is the upper limit of the angular frequency in the wind fluctuation, $S(\omega)$ is the auto-power spectrum density function, and $S(\omega)$ <1. The increase in frequency is:

$$\Delta\omega = \frac{(\omega_u - \omega_s)}{N}, \tag{16}$$

in which, $\Delta\omega$ is frequency increment; N represents the divisor of fluctuating wind frequency. To increase the period of the simulated sample, Shinozuka [26] suggested that

$$\omega_k = k\Delta\omega_k - \frac{N-l}{N}\Delta\omega_k = (k-1)\Delta\omega_k + \frac{l}{N}\Delta\omega_k. \tag{17}$$

Here, N should be a sufficiently large positive integer to avoid distortion. The time increment of the simulated time series can be determined in the following ways:

$$\Delta t = \frac{T_0}{M} = \frac{2\pi}{M\Delta\omega} = \frac{2N}{M} \times \frac{\pi}{\omega_u}. \tag{18}$$

The number of samples in the simulation time series is M, where M is an integer, and M should be greater than 2N; and the time increment should be small enough, Ensure that $\Delta t \leq \pi/\omega_u$.

2.3. Wind-Sand Loads Applied to the Transmission Tower. The dynamic response of the transmission tower subjected to a sandstorm can be analyzed as the response of the tower to wind loads and sand loads, similarly to the wind-rain effect [27, 28]. Thus, the load per unit volume F experienced by the transmission tower structure can be calculated as follows:

$$F = F_w + F_s, \tag{19}$$

where F_w represents the wind load per unit volume and F_s the sand load per unit volume.

The along-wind loads are calculated by:

$$F_w(t) = \frac{\mu_s A v_s(t)^2}{1.6}, \tag{20}$$

where A is the area acted on by wind, μ_s is the shape coefficient, and $v_s(t)$ is the wind speed.

Substitution of (10) and (20) into (22) yields:

$$F(t) = F_w(t) + F_s(t) = \frac{\mu_s A v_s(t)^2}{1.6 + 4\rho_{TSP} v_s(t)^2 A}. \tag{21}$$

3. FE Model of the Transmission Tower-Line System and the Wind-Sand Loads

3.1. Structural Model of Transmission Tower. The prototype tower of this study is the SZ27104J straight-line tower (Figure 2), with a height of 123.6 m, a width of 24.48 m, and a typical horizontal span length of 400 m. The structure is constructed mainly from Q235 and Q345 steel pipes and angle irons with an elastic modulus of 206 GPa. According to the linear tower model in SAP2000, the overall control parameters of the model in MATLAB are determined. This article takes the SJ27103JD linear tower as the engineering background. The linear tower finite element model contains 306 nodes, 888 members, 41 cross section types, 4 boundary conditions, and 1836 degrees of freedom members are made of Q345 steel, while the auxiliary members are made of Q235 steel. The dimensions of the main cross-sections of the linear tower are marked in Figure 2. In Figure 2, R-means round steel pipe, and L-means angle steel. The tower-line system (Figure 3) consists of 4 self-supporting towers and 5 spans. Each span is composed of three levels of eight-bundle conductors and optical ground wires (OPGW), of which the model number and specifications are listed in

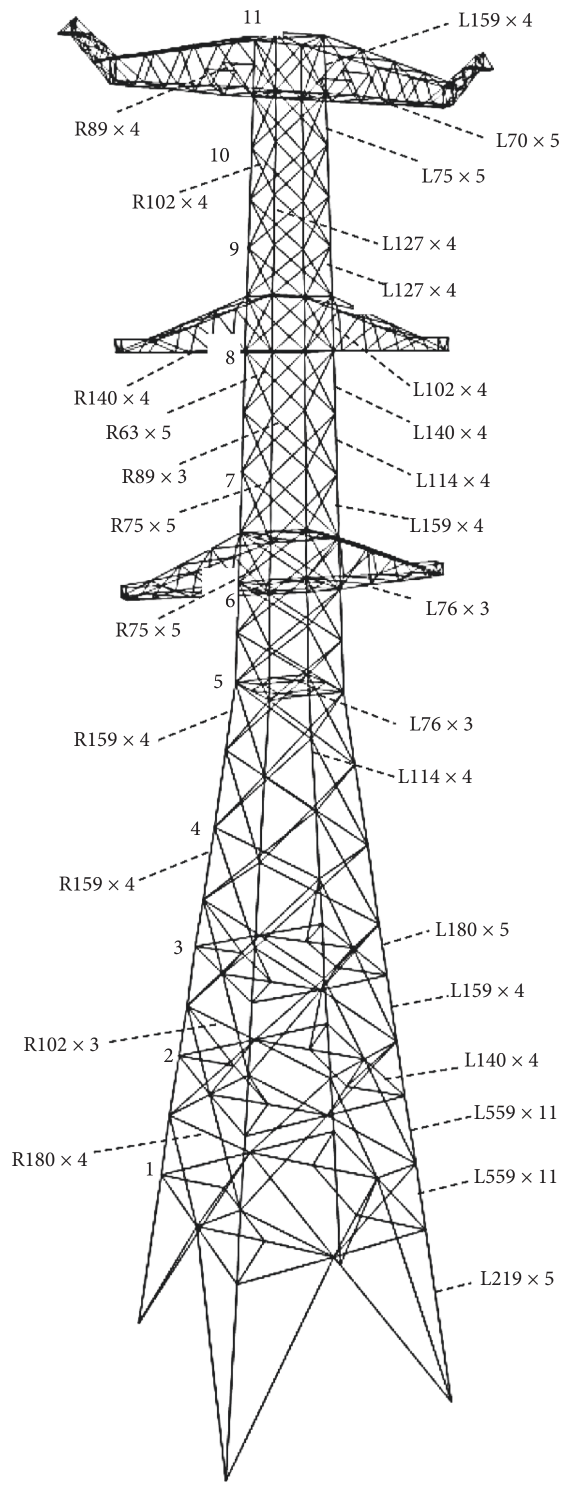

Figure 2: The finite element model of the SZ27104J linear tower and the dimensioning of its section.

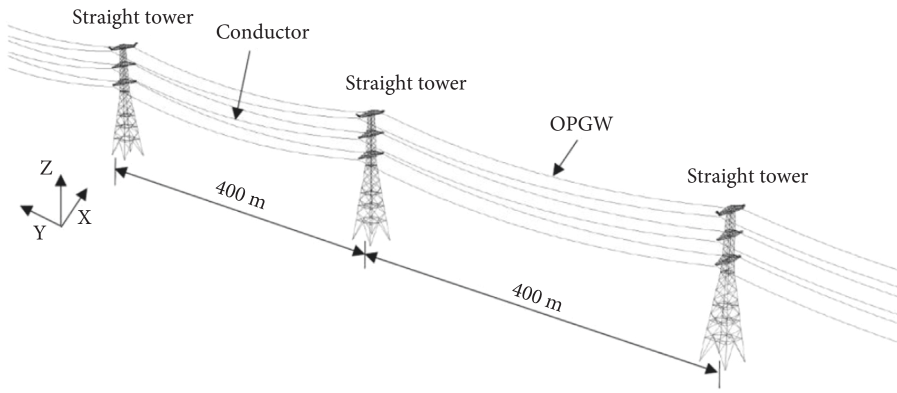

Figure 3: Model of the transmission tower-line system established in SAP2000.

Table 2: Specification of conductors and OPGW.

Type	Conductor	OPGW
Line model number	JL1/LHA1-465/210	OPGW-185
Cross section area	673.73 mm^2	184.38 mm^2
Diameter	33.75 mm	18.2 mm
Mass per unit length	1.8642 kg/m	1.256 kg/m
Tensile capacity	130169 N	211700 N
Elastic modulus	55000 N/mm^2	162000 N/mm^2
Thermal expansion coefficient	23×10^{-6}°C	13×10^{-6}°C
Bundle number	8	1

Table 2. Simulations were conducted using the finite element software SAP2000.

3.2. Wind-Sand Load Simulation. In this paper, Kaimal fluctuating wind energy spectrum and harmonic superposition method are used to simulate wind load in MATLAB. According to Table 1, the average wind speed $V10$ at a height of 10 m is set to 3 m/s, 6 m/s, 10 m/s, 15 m/s, 20 m/s, and 25 m/s. When the average wind speed V_{10} of the transmission tower at a height of 10 m is set to 3 m/s, 6 m/s, and 10 m/s, the response value of the linear tower-line system under the action of wind-sand load and pure wind load does not exceed the difference 1.54%, so in the analysis in Section 4, only wind speeds of 15 m/s, 20 m/s, and 25 m/s are selected to act on the linear tower-line system.

The foundation flexibility in desert conditions may highly affect dynamic structural response compared to standard subsoil foundations. There are a large number of nodes in the transmission tower, so it is impossible to perform a time history analysis of the wind speed at each node in the transmission tower. Since it is necessary to analyze the dynamic response of the entire transmission tower-line system under wind load conditions, it is also necessary to determine the point of action of the wind load on the conductor in the tower-line system. According to Figure 4, the transmission tower is simplified to 11-layer mass points. Figure 4 shows the simplified number and number of nodes in the straight-line tower. The other

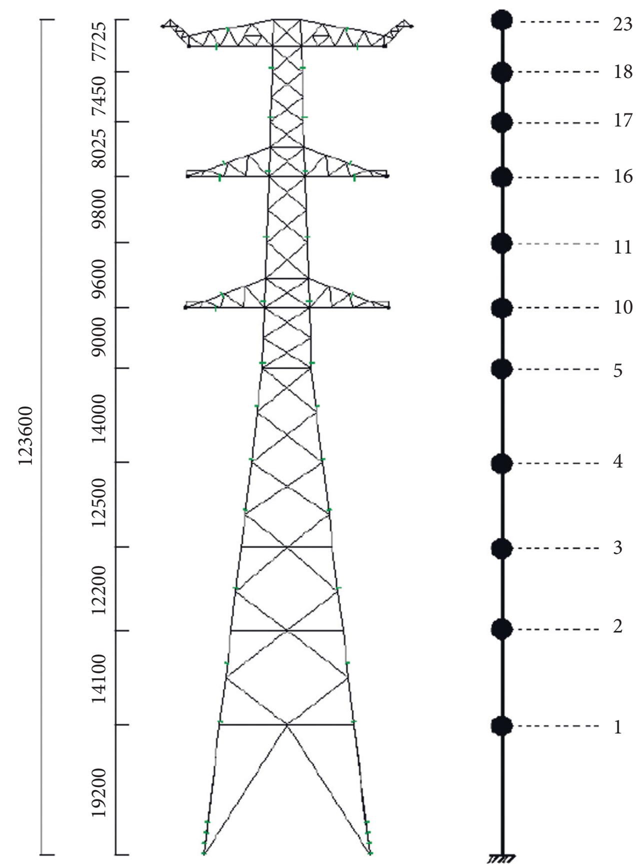

Figure 4: Wind simulation points.

numbers not shown in Figure 4 are simplified mass points selected on the wire; therefore, the straight-line tower-line system is divided into 23 mass point regions in total. The position of the load and the windward areas are listed in Table 3.

In order to simulate wind loads in MATLAB, the parameters of the wind speed time history model need to be determined.

The simulation coverage interval is 8.3 min, the frequency of wind speed fluctuation is f_s, and the value range is 0.1~100 Hz. Due to:

Table 3: The positions of wind load and windward areas.

Point	Height (m)	Area (m^2)	Point	Height (m)	Area (m^2)	Point	Height (m)	Area (m^2)
1	19.20	35.63	9	76.32	0.03	17	103.09	0.18
2	33.30	22.13	10	81.00	19.49	18	105.07	0.13
3	45.50	17.14	11	83.89	0.18	19	108.43	4.96
4	58.00	16.19	12	85.87	0.13	20	109.02	0.08
5	64.49	0.18	13	89.82	0.08	21	114.92	0.03
6	66.47	0.13	14	90.60	7.49	22	115.88	4.41
7	70.42	0.08	15	95.72	0.03	23	123.60	13.42
8	72.00	13.79	16	100.40	15.84			

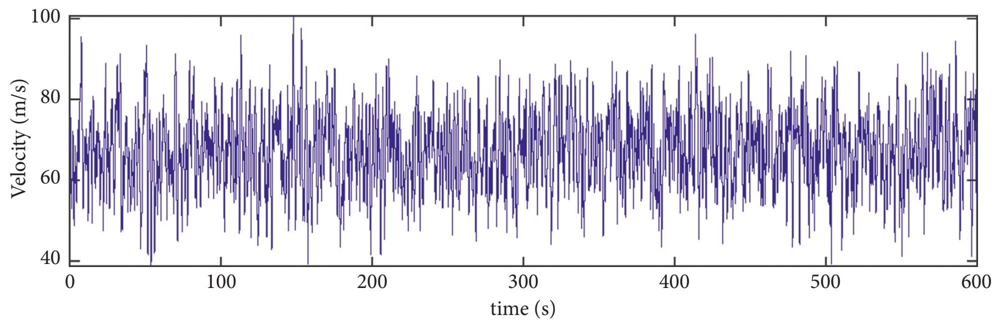

Figure 5: The time history of wind speed at the top of the tower, $V_{10} = 25$ m/s.

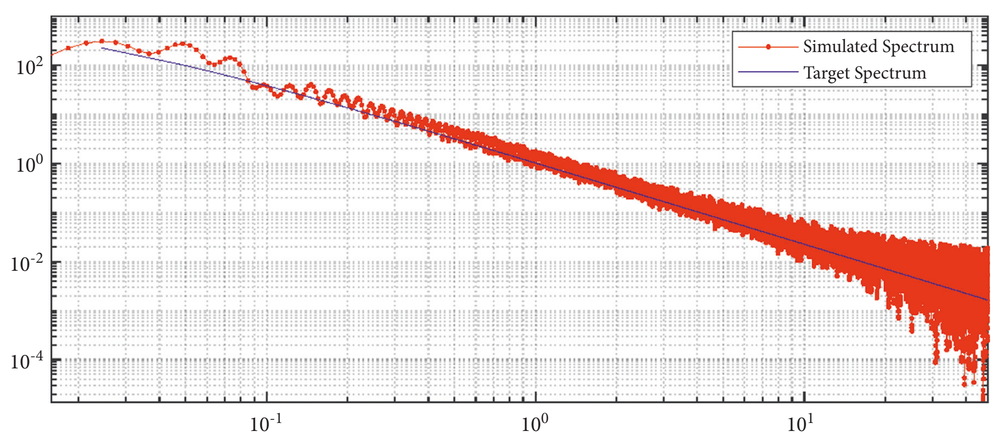

Figure 6: Power spectral comparison at the top of the tower, $V_{10} = 25$ m/s.

$$\mathrm{d}t = \frac{1}{f_s}. \tag{22}$$

To capture higher frequency fluctuations in the wind, the f_s value is 100 Hz, so the time interval dt is 0.01 s. Figure 5 shows the simulated wind speed at the top of the tower, when the wind speed at 10 m, $V_{10} = 25$ m/s. The turbulence intensity in this situation is 0.366. Figure 6 shows the power spectrum density of the simulated fluctuating wind compared to the target spectrum.

4. Dynamic Response Analysis of the Tower-Line System under Wind-Sand Load

The dynamic response of the power transmission tower-line system can be obtained by the following motion equation:

$$[\mathbf{M}]\{\ddot{x}(\mathbf{t})\} + [\mathbf{C}]\{\dot{x}(\mathbf{t})\} + [\mathbf{K}]\{\mathbf{x}(\mathbf{t})\} = \{\mathbf{P}(\mathbf{t})\}, \tag{23}$$

where $[\mathbf{M}]$, $[\mathbf{C}]$, and $[\mathbf{K}]$ represent structural mass, damping and stiffness matrices, respectively; $\{\ddot{x}(\mathbf{t})\}$, $\{\dot{x}(\mathbf{t})\}$, and $\{\mathbf{x}(\mathbf{t})\}$ are the acceleration, velocity, and displacement vectors, respectively; $\{\mathbf{P}(\mathbf{t})\}$ is the vector of the loads generated by (20) (pure wind load) or (10) (wind-sand load). In this study, six levels of wind-sand loads are generated based on the parameters of the sandstorms, as listed in Table 1. Pure wind loads are also generated to compare the increasement of dynamic response. In equation (24), the damping matrix $[\mathbf{C}]$ can be expressed in the form of Rayleigh damping, assuming that the modal damping ratio is 2%, according to the design manual.

It should be noted that the stiffness of the wire is a time-varying parameter, since it depends on the time-varying shape of the wire (also known as geometric nonlinearity). Therefore, the nonlinear time-domain analysis shall be performed to

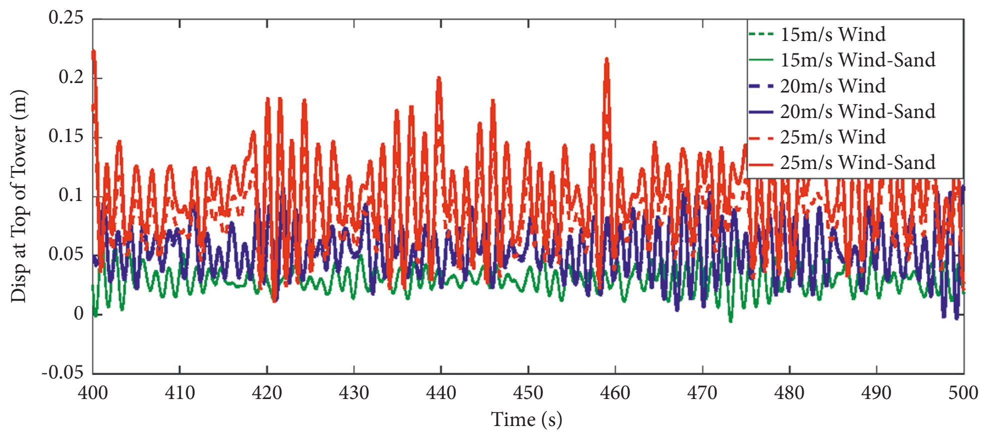

Figure 7: Displacement at the top of tower 2#.

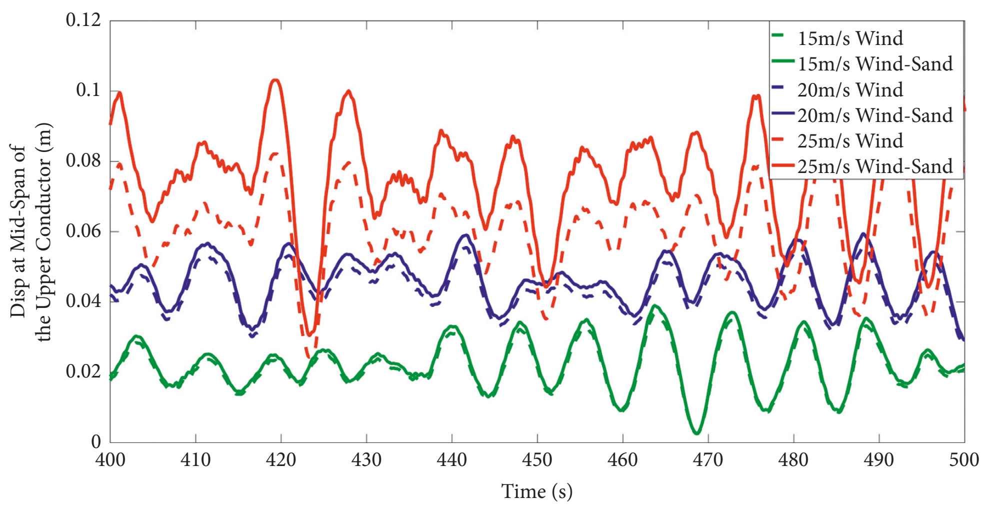

Figure 8: Displacement at the mid-span of the upper conductor.

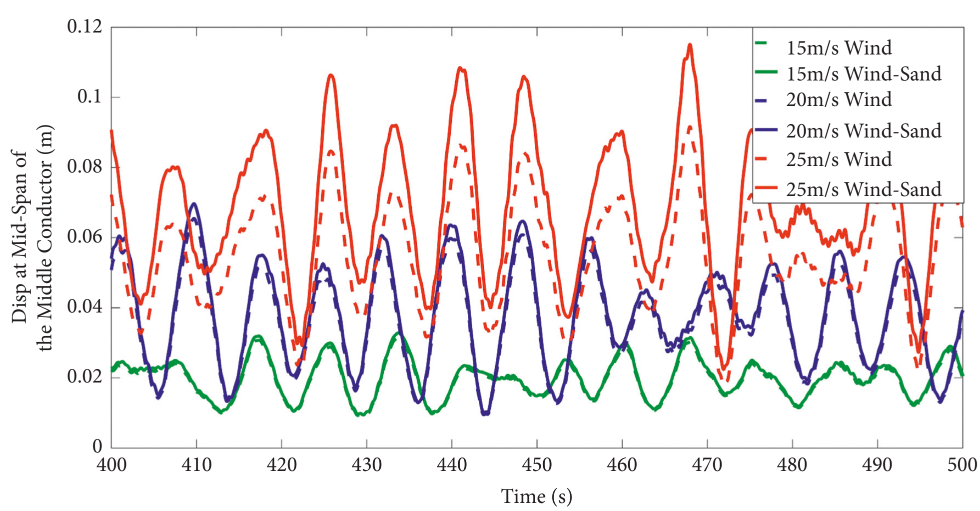

Figure 9: Displacement at the mid-span of the middle conductor.

acquire accurate results for the power transmission tower-line system. The direct integration method embedded in SAP2000 was utilized to solve (21) with the P-Delta effect and large displacement is considered. Hilber–Hughes–Taylor (HHT) method is selected as the time integration method and other parameters are set to the default value of SAP2000.

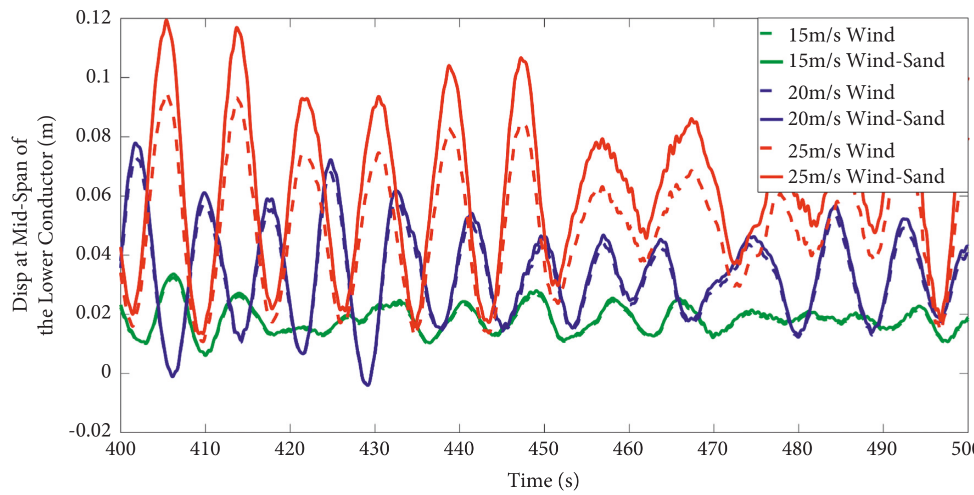

Figure 10: Displacement at the mid-span of the lower conductor.

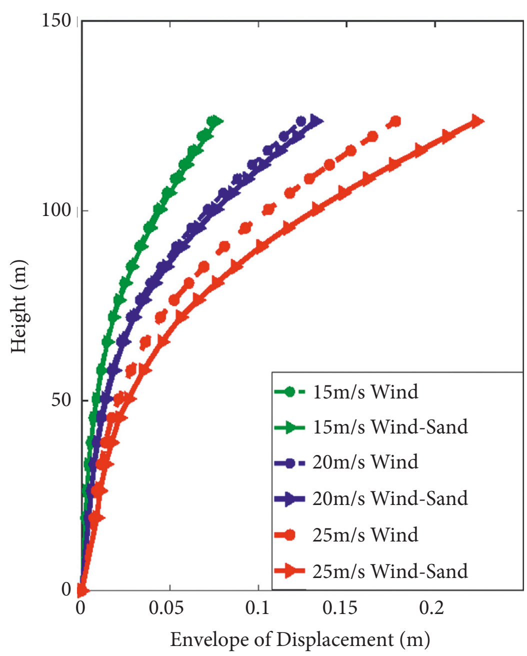

Figure 11: Displacement envelope.

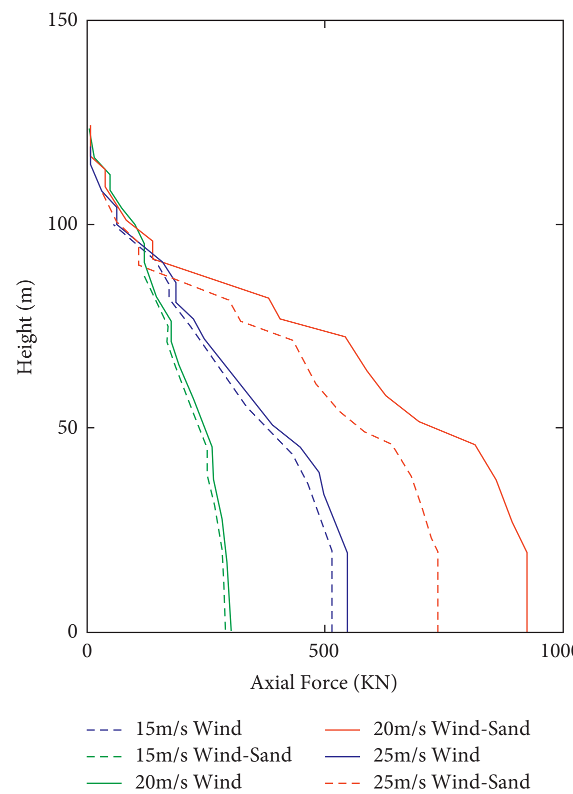

Figure 12: Axial force envelope.

The time step selected for the dynamic time history is dt = 0.01, and the interception time of the time history graph is 6.7 min–8.3 min.

For the time history diagram of tower top displacement in Figure 7, the amplitude range is 0–0.25 m. At this time, the frequency of the fluctuation of the tower top displacement is larger, and a denser fluctuation curve is obtained.

Observing Figure 8, the displacement value of the uppermost conductor in the tower-line system at 15–25 m/s wind speed ranges from 0 to 0.12 m, and the maximum displacement fluctuation range is at 25 m/s wind speed.

Observing Figure 9, the displacement of the middle layer of the tower-line system is still 0~0.12 m when the wind speed is 15–25 m/s. And the displacement fluctuation range at each wind speed is more obvious than that of the upper conductor, and the displacement amplitude is the largest at a wind speed of 25 m/s.

Observing Figure 10, the displacement value of the bottom conductor in the tower-line system at the wind speed of 15–25 m/s is still 0–0.12 m. At this time, the amplitude of the displacement at the wind speed of 25 m/s and the wind speed of 15 m/s are both larger than the amplitude at 15 m/s.

Comparing Figures 8–10 with Figure 7, it can be seen that the displacement fluctuation frequency of the mid-span node of the wire is smaller than that of the tower top node

Table 4: Dynamic response value and growth rate.

Dynamic response	Load cases	Floating dust	Blowing sand	Sandstorm			
				Weak	Medium	Strong	Extra strong
Displacement at tower top (mm)	Wind	2.92	11.72	32.61	73.498	124.18	177.72
	Wind-sand	2.93	11.75	33.11	76.32	155.97	223.22
	Increment	0.08%	0.26%	1.54%	3.84%	6.40%	25.60%
Acceleration at the tower top (m/s^2)	Wind	0.1	0.41	1.12	2.51	4.45	6.95
	Wind-sand	0.1	0.41	1.13	2.61	4.73	8.7292
	Increment	0.08%	0.26%	1.54%	3.84%	6.40%	25.60%
Max. axial force (kN)	Wind	1.16	4.65	12.96	29.24	51.61	73.92
	Wind-sand	1.16	4.66	13.16	30.36	64.82	92.84
	Increment	0.08%	0.26%	1.54%	3.84%	6.40%	25.60%
Max. disp. of upper conductor (mm)	Wind	1.29	5.67	16.96	40.49	76.72	113.54
	Wind-sand	1.29	5.68	17.22	50.86	81.63	142.61
	Increment	0.08%	0.26%	1.54%	3.84%	6.40%	25.60%
Max. disp. of middle conductor (mm)	Wind	1.32	5.94	18.06	43.64	71.81	119.44
	Wind-sand	1.32	5.96	18.34	45.32	76.4	150.02
	Increment	0.08%	0.26%	1.54%	3.84%	6.40%	25.60%
Max. Disp. of lower conductor (mm)	Wind	1.3	5.43	15.58	35.94	73.19	111.51
	Wind-sand	1.3	5.44	15.82	37.32	77.87	140.06
	Increment	0.08%	0.26%	1.54%	3.84%	6.40%	25.60%

under the same period of time and the same wind speed, and other conditions are the same.

The numerical results are presented in Figures 7–12. It can be observed that as the wind speed increases, the wind-sand coupling effect is more obvious. In Figure 7, for instance, when the wind speed is 15 m/s (corresponding to the medium sandstorm according to Table 1), the displacement response at the top of Tower 2 under pure wind excitation is identical to that under the wind-sand load. When the wind speed reaches 25 m/s (extra strong sandstorm), the displacement of the displacement is amplified. A similar trend can also be observed in Figures 8–10, which display the displacement at the mid-span of the three levels of conductors.

Figures 11 and 12 present the envelope of displacement and axial forces of the main members along the height of the tower. These curves indicate that the internal forces are amplified by the wind-driven sands.

In Table 4, the responses under all the six levels of sandstorms and pure winds are compared. It is obvious that the displacements, accelerations, and internal forces of key structural members are all increased, especially under the extra strong sandstorms, when the responses are increased by 25.6%. Therefore, it is suggested that the wind-sand load be considered in future design codes of transmission tower-line systems.

The maximum displacement of the mid-span node of the middle-level conductor is greater than the maximum mid-span displacement of the upper conductor, and the mid-span node of the bottom conductor fluctuates most obviously at a wind speed of 25 m/s. The maximum displacement of the mid-span node on the traverse is similar for each layer, the maximum displacement of the tower top is 223.22 m, and the growth rate under the state of sand particles and pure wind at various wind speeds maintains a stable law.

5. Conclusions

This paper presents an analysis method of transmission tower-line system under wind-sand load. According to the law of conservation of momentum, the impact force generated by a single sand particle hitting the steel structure is derived. Then the wind-sand load is simulated with the help of graded sand-dust storm intensity. An actual transmission tower-line system was established in SAP2000 to realize time-domain analysis. Some conclusions revealed by the data results are summarized as follows:

(1) Besides the erosion actions and corona effects, the floating sand particles in wind will also amplify the dynamic response of the power transmission tower-line system. Neglecting this amplification effect, which is commonly applied in the current design procedure may underestimate the potential danger of the sandstorm.

(2) The wind-sand loads are determined by the wind speed and the ratio of the sand particles floating in the air. As the sandstorm level increases, the wind-sand load grows rapidly.

(3) Compared to the dynamic response from wind-induced loads, the nonlinearity of the tower dynamic response increased clearly under increasing levels of the sandstorm intensity. The higher the sandstorm level, the greater the displacement of the top tower and axial force experienced by the principal material. Under extreme conditions, i.e., the extra strong sandstorm, the response can be increased by 25%. Therefore, an amplification factor of 1.25 is suggested to consider the influence of the wind-driven sand for future design codes.

In addition, field observation or long-term health monitoring shall be conducted to further reveal the intensity of wind storms and their influence on the response of the tower-line system in future work.

Data Availability

The data used to support the findings of this study are available from the corresponding author upon request.

Conflicts of Interest

The authors declare that there are no conflicts of interest regarding the publication of this paper.

Acknowledgments

This research was funded by the National Natural Science Foundation of China (NSFC), grant number 51808092, the United Navigation Foundation of Liaoning Province, grant number 2020-HYLH-48, the National Key Research and Development Program of China (2021YFB2601102), and the Open Fund of the State Key Laboratory of Coastal and Offshore Engineering (DUT-LP2122).

References

[1] Y. He, Z. Gu, Q. Shui et al., "RANS simulation of local strong sandstorms induced by a cold pool with vorticity," *Atmosphere*, vol. 11, no. 4, p. 321, 2020.

[2] M. Yang, Y. Wang, Q. Liu, A. Ding, and Y. Li, "The influence of sandstorms and long-range transport on polycyclic aromatic hydrocarbons (PAHs) in PM2.5 in the high-altitude atmosphere of southern China," *Atmosphere*, vol. 6, no. 11, pp. 1633–1651, 2015.

[3] JM. Prospero, P. Ginoux, O. Torres, S. E. Nicholson, and T. E. Gill, "Environmental characterization of global sources of atmospheric soil dust identified with the NIMBUS 7 Total Ozone Mapping Spectrometer (TOMS) absorbing aerosol product," *Review of Geophysics*, vol. 40, no. 1, pp. 2-1–2-31, 2002.

[4] Z. Qian, X. Lu, and S. Ding, "Full-scale tests on pad and chimney foundation subject to uplift combined with horizontal loads in aeolian sand," *Yantu Lixue/Rock and Soil Mechanics*, vol. 30, pp. 257–260, 2009.

[5] B. Yang, Y. Wang, and J. Liu, "PIV measurements of two phase velocity fields in aeolian sediment transport using fluorescent tracer particles," *Measurement*, vol. 44, no. 4, pp. 708–716, 2011.

[6] DJ. Sherman and B. Li, "Predicting aeolian sand transport rates: a reevaluation of models," *Aeolian Research*, vol. 3, no. 4, pp. 371–378, 2012.

[7] G. Strypsteen, L. C. Van Rijn, and P. Rauwoens, "Comparison of equilibrium sand transport rate model predictions with an extended dataset of field experiments at dry beaches with long fetch distance," *Aeolian Research*, vol. 52, Article ID 100725, 2021.

[8] P. Zhang, D. J. Sherman, and B. Li, "Aeolian creep transport: a review," *Aeolian Research*, vol. 51, Article ID 100711, 2021.

[9] Z. Zheng, S. Du, H. Taubenbock, and X. Zhang, "Remote sensing techniques in the investigation of aeolian sand dunes: a review of recent advances," *Remote Sensing of Environment*, vol. 271, Article ID 112913, 2022.

[10] Q. Gao and YH. Shi, "Research on the mechanism of discharge of transmission line in wind-sand-electric field," *Applied Mechanics and Materials*, vol. 43, pp. 169–172, 2010.

[11] L. Yunpeng, H. Feng, L. Chen et al., "Corona loss of the bundle conductors on EHV/UHV AC power lines under sandy and dusty conditions in high-altitude areas," *J Electrostat*, vol. 107, Article ID 103476, 2020.

[12] M. F. Ishac and H. B. White, "Effect of tornado loads on transmission lines," *IEEE Transactions on Power Delivery*, vol. 10, no. 1, pp. 445–451, 1995.

[13] R. V. Milford and A. M. Goliger, "Tornado risk model for transmission line design," *Journal of Wind Engineering and Industrial Aerodynamics*, vol. 72, pp. 469–478, 1997.

[14] E. Savory, G. A. R. Parke, M. Zeinoddini, N. Toy, and P. Disney, "Modelling of tornado and microburst-induced wind loading and failure of a lattice transmission tower," *Engineering Structures*, vol. 4, pp. 365–375, 2001.

[15] S. E. Oliver, W. W. Moriarty, and J. D. Holmes, "A risk model for design of transmission line systems against thunderstorm downburst winds," *Engineering Structures*, vol. 9, pp. 1173–1179, 2000.

[16] C. Q. Li, "A stochastic model of severe thunderstorms for transmission line design," *Probabilistic Engineering Mechanics*, vol. 4, pp. 359–364, 2000.

[17] A. Shehata, A. El Damatty, and E. Savory, "Finite element modeling of transmission line under downburst wind loading," *Finite Elements in Analysis and Design*, vol. 1, pp. 71–89, 2005.

[18] SA. Orr and M. Cassar, "Exposure indices of extreme wind-driven rain events for built heritage," *Atmosphere*, vol. 11, no. 2, p. 163, 2020.

[19] Y. Hao, Y. Liao, Z. Kuang et al., "Experimental investigation on influence of shed parameters on surface rainwater characteristics of large-diameter composite post insulators under rain conditions," *Energies*, vol. 13, no. 19, p. 5011, 2020.

[20] A. An, G. Guan, Z. Zhu, and Y. Zhang, "Research on windage Yaw Flashovers of transmission lines under wind and rain conditions," *Energies*, vol. 12, no. 19, p. 3728, 2019.

[21] C. Zhou, J. Yin, and Y. Liu, "Large swing behavior of overhead transmission lines under rain-load conditions," *Energies*, vol. 11, no. 5, p. 1092, 2018.

[22] T. Li, *Approaches and Dynamic Performances of High-Speed Train Fluid-Structure. PhD*, Southwest JiaoTong University, Chengdu, China, 2012.

[23] J. Cheng, F. Jiang, C. Xue, and Q. Pang, "Computational method for maximum sediment discharge and sand-carrying wind load in the prevention and treatment of wind drift sand for railway in strong wind area," *Zhongguo Tiedao Kexue/China Railway Science*, vol. 33, pp. 1–5, 2012.

[24] F. Jiang, Y. Li, K. Li, J. Cheng, C. Xue, and S. Ge, "Study on structural characteristics of Gobi wind sand flow in 100 km wind area along Lan-Xin Railway," *Tiedao Xuebao/Journal of the China Railway Society*, vol. 32, pp. 105–110, 2010.

[25] M. Shinozuka and CM. Jan, "Digital simulation of random processes and its applications," *Journal of Sound and Vibration*, vol. 25, no. 1, pp. 111–128, 1972.

[26] M. Shinozuka and G. Deodatis, "Simulation of stochastic processes by spectral representation," *Applied Mechanics Reviews*, vol. 44, no. 4, pp. 191–204, 1991.

[27] X. Fu, HN. Li, and J. Wang, "Failure analysis of a transmission tower subjected to combined wind and rainfall excitations," *The Structural Design of Tall and Special Buildings*, vol. 28, no. 10, 2019.

[28] X. Fu and G. Li, "Fragility analysis of a transmission tower under combined wind and rain loads," *Journal of Wind Engineering and Industrial Aerodynamics*, vol. 199, Article ID 104098, 2020.